

# MODELLING OF THE INFLUENCE OF ELECTROMAGNETIC FORCE ON MELT CONVECTION AND DOPANT DISTRIBUTION DURING FLOATING ZONE GROWTH OF SILICON

SABANSKIS<sup>1</sup> A., SUROVOVS<sup>1,2</sup> K., KRAUZE<sup>1</sup> A., PLATE<sup>1</sup> M., VIRBULIS<sup>1</sup> J.

<sup>1</sup>Faculty of Physics and Mathematics, University of Latvia, 8 Zellu str., LV-1002, Riga, Latvia

<sup>2</sup>Institute of Solid State Physics, University of Latvia, 8 Kengaraga str., LV-1063, Riga, Latvia

E-mail address of corresponding author: [andrejs.sabanskis@lu.lv](mailto:andrejs.sabanskis@lu.lv)

**Abstract:** Numerical modelling of floating zone process is considered. A local analysis of the electromagnetic (EM) field distribution near the external triple point (ETP) was carried out and the result was included in the calculation of phase boundaries, to improve the surface current formulation. 3D hydrodynamic calculations were performed using the open source code library *OpenFOAM*. The influence of high-frequency EM field is shown by comparing phase boundaries, convection in melt and radial resistivity variation profiles. The results are compared with experimental data.

## 1. Introduction

The floating zone (FZ) method is applied for growth of silicon (Si) single crystals appropriate for power electronics (high purity crystals), because molten silicon is not in contact with other materials. High-frequency (HF) inductor is used to melt silicon feed rod with induced currents. Molten silicon flows downwards and crystallizes due to radiative heat losses. Numerical modelling is used for process development due to its inexpensiveness and possibility to reveal aspects that cannot be observed directly, e.g. hydrodynamics (HD) in melt. It is crucial to describe EM field as precisely as possible, because it influences the shape of phase boundaries as well as convection and dopant transport in melt. From the dopant field it is possible to obtain radial resistivity variation (RRV) in grown single crystal [1]. The models can be validated using experimental RRV measurements.

In the present work the precision of calculation of EM field is improved introducing a correction near triple points and verified by comparison with experiment. The influence of the EM field on phase boundaries, melt convection and dopant distribution in melt is presented and discussed. Main physical fields in melt are analysed, the shape of crystallization interface and RRV profiles are compared to experimental data [2].

## 2. Mathematical models and software

**2.1. Phase boundaries.** 2D axisymmetric calculations of phase boundaries are carried out using a specialized program *FZone* [3]. Since the skin depth varies between 0.038 mm for the copper inductor and 1.3 mm for the solid silicon, much less than the characteristic dimensions of the FZ system ( $\approx 0.1$  m), the EM field distribution is determined by surface current density. HF EM field is calculated considering the 3D HF inductor [4]. 3D induced surface power density values are azimuthally averaged and included in 2D axisymmetric phase boundary calculations as a heat source. From the temperature field and heat balance equations, the direction and magnitude of the movement of each interface point are obtained, and the quasi-stationary shape of phase boundaries is found iteratively [3].

**2.2. EM correction near electrical resistivity jump.** The HF approximation, which is described in [3], cannot be used when the exact distribution of volumetric EM field is important – for example, in the vicinity of solid-liquid interface, where skin depth changes 5 times. A local analysis of the EM field distribution in the vicinity of external triple point was carried out

using the complex vector potential formulation. It was shown that in the first few millimetres near the ETP the actual induced power is significantly differs from the HF approach: more power is induced in the melt and less in the crystal, see Figure 1. The result of local analysis was included in *FZone* as correction to EM heat sources at free melt and crystal side surfaces. Because of changed EM heat sources in crystal and melt, inductor current needs to be adjusted to maintain the same zone height. The crystallization interface shape near the ETP changes due to local heat source changes; global shape changes occur because of different inductor current and integral induced power on free melt surface.

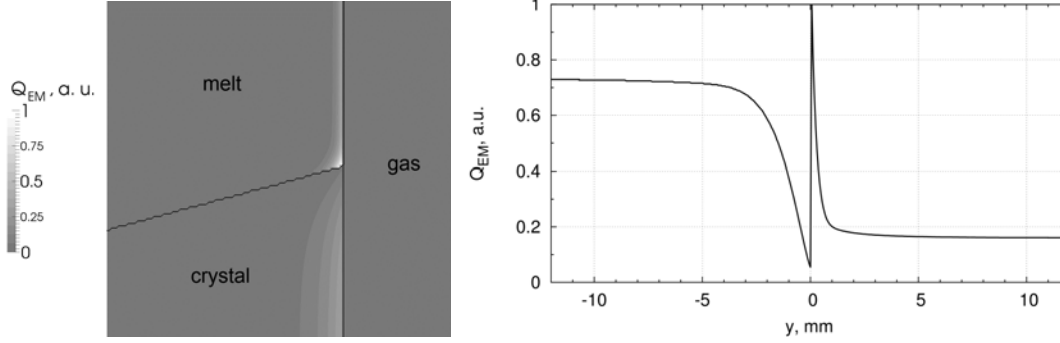


Figure 1: Left: induced EM power density distribution in the vicinity of ETP, arbitrary units. Right: linear induced EM power, arbitrary units.  $y > 0$  corresponds to melt,  $y < 0$  – to crystal.

**2.3. 3D melt flow.** The unsteady 3D melt flow in the FZ process is modelled using the open source code library *OpenFOAM*. For the considered system Reynolds number is roughly 1500, therefore the melt flow is considered as laminar. The detailed description of the mathematical model is given in [1], only the details relevant to the present study are summarized.

For incompressible melt flow, Navier-Stokes equations are solved, and for description of buoyancy, Boussinesq approximation is used. The crystallization interface is considered as velocity outlet with the boundary conditions for velocity that include constant mass flow and rotation. The melting interface is considered as inlet. The Marangoni force distribution (obtained from temperature field) and tangential to surface EM force distribution acquired from the 3D HF EM calculations are used for boundary conditions for the melt velocity on the

free melt surface:  $f = \frac{1}{4} \mu_0 \delta \nabla_s j^2 + M \nabla_s T$ , where  $f$  is surface force,  $\delta = \frac{1}{\sqrt{\pi f_{ind} \sigma \mu_0}}$  is skin

depth,  $\nabla_s$  is surface gradient,  $j$  is surface current density,  $M = -1.3 \cdot 10^{-4}$  N/(m K) is Marangoni

coefficient,  $T$  is temperature,  $f_{ind}$  is inductor current frequency and  $\sigma$  is conductivity of liquid silicon. Marangoni force is directed from higher to lower temperatures, EM force,  $F_{EM}$ , – typically in the opposite direction. Temperature field is governed by non-stationary convection-diffusion equation. Boundary conditions are: fixed temperature, equal to melting point of Si, on melting and crystallization interfaces; fixed heat flux density, equal to sum of radiative heat losses and EM induced power density, on melt free surface. For the dopant concentration field,  $C$ , the mass transport equation is solved. From the calculated  $C$  distribution at the crystallization interface the resistivity of grown crystal,  $\rho$ , can be obtained:  $\rho = 1/k_0 C$ , where  $k_0$  is the segregation coefficient.

### 3. Calculation results

Phase boundaries of the considered 4" FZ system (information about IKZ Berlin system parameters and geometry of inductor can be found in [2]) are calculated using program *FZone* and shown in Figure 2 on the left. When EM correction at ETP is included, higher inductor current is required to hold prescribed zone height (32.5 mm) and it leads to larger deflection of crystallization interface. This shape is closer to the experimental one. Induced EM power density and force density vectors for different inductor current frequency are in Figure 2 on the right. Heat sources are approximately the same, because calculation algorithm is maintaining fixed zone height.  $F_{EM}$  is slightly different: maximal values are  $0.49 \text{ N/m}^2$  for 3 MHz and  $0.57 \text{ N/m}^2$  for 2 MHz.

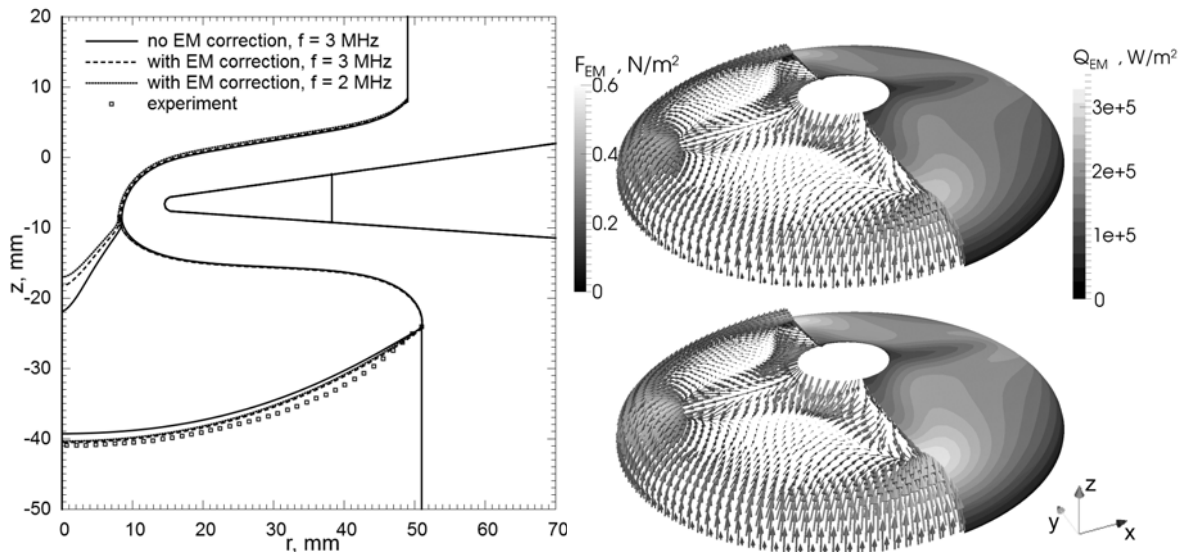


Figure 2: Left: phase boundaries of considered system for various EM fields. Right: EM heat sources and EM force on free melt surface for cases with EM correction for different inductor current frequency (top – 3 MHz, bottom – 2 MHz). Current suppliers are in +x direction.

Using the obtained axisymmetric shape of phase boundaries, 3D HD calculations were performed on a block-structured mesh consisting of 80000 hexahedral elements. A sample of calculated fields – melt velocity, temperature and dopant concentration – is shown in Figures 3 and 4. Characteristic temperature maxima are formed below the additional slits of inductor due to non-symmetric induced heat sources (see Figure 2). Velocity field shows that near the ETP EM forces are dominating and creating a distinct vortex directed upwards.

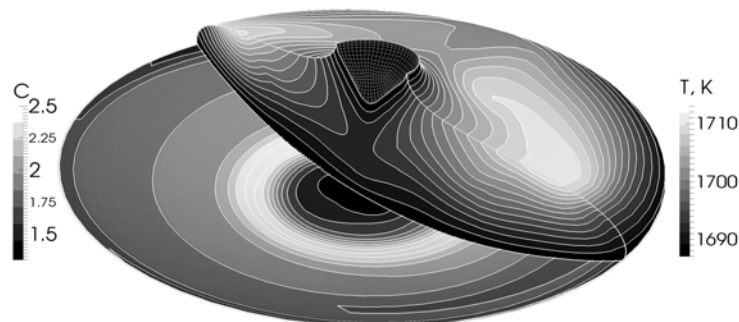


Figure 3: Crystallization interface and vertical cut of the melt. Melt temperature is shown in the right part of melt; dopant concentration is depicted on crystallization interface.

Calculation example with EM correction and  $f_{ind} = 3 \text{ MHz}$ .

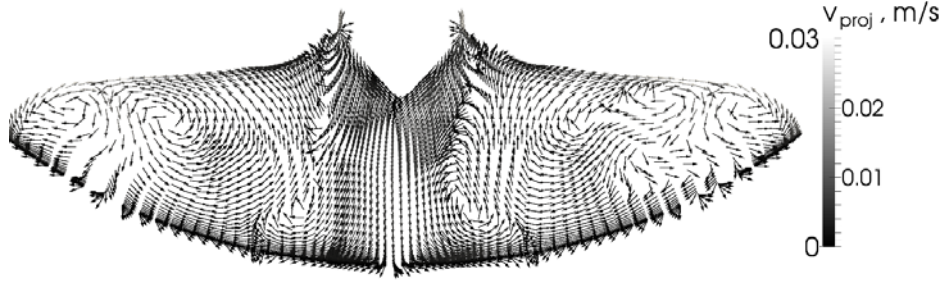


Figure 4: Time-averaged melt velocity projection on the vertical slice of the melt, perpendicular to inductor current suppliers,  $f_{ind} = 3$  MHz.

To investigate the influence of EM forces on melt motion more precisely, distribution of tangential melt velocity component (projected on the plane of the slice) is shown in Figure 5. The case where EM force is not considered differs considerably from other cases which are very similar despite to different EM forces for frequency of 2 and 3 MHz. It can be explained with increased temperature gradients in 2 MHz case (maximum temperature increased from 1712 to 1720 K) causing larger Marangoni forces which are compensating the increased EM forces in this case (see temperature distribution in Figure 6), which compensate changes in EM force. Finally, from concentration distribution on crystallization interface RRV profiles are obtained (see Figure 7). The sum of squared differences between experimental and calculated RRV profiles in Table 1 shows that the case with EM correction and  $f_{ind} = 3$  MHz describes experimental data more precisely than others. Experimental data was obtained using  $f_{ind} = 3$  MHz, and the expected result that calculation with  $f_{ind} = 2$  MHz has a worse agreement with experiment indicates that the used system of numerical models is sensitive to inductor current frequency.

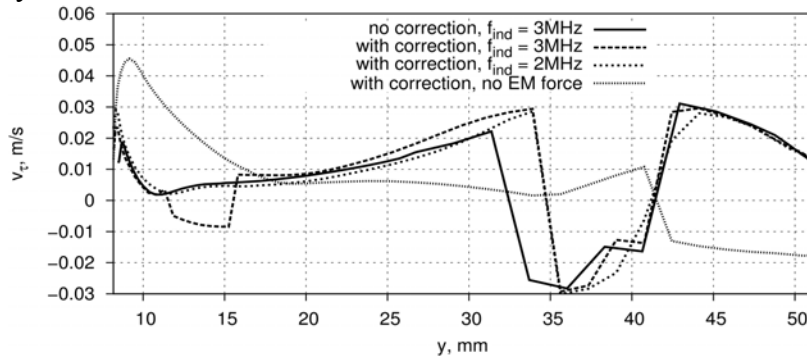


Figure 5: Distribution of in-plane velocity on melt free surface.  $y$  is horizontal coordinate perpendicular to inductor current suppliers, 51 mm corresponds to ETP.

$v_\tau$  is defined as positive if melt moves towards the crystal axis.

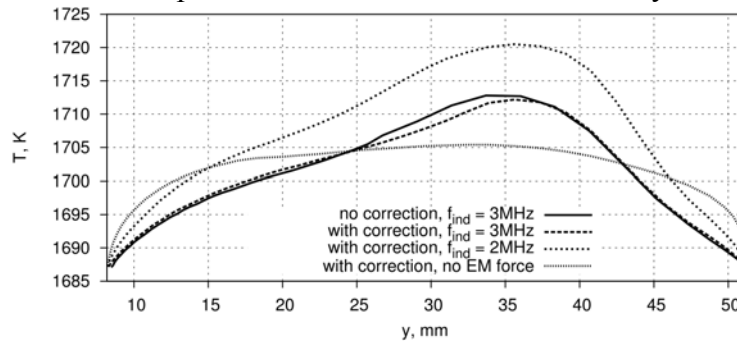


Figure 6: Distribution of temperature on melt free surface.  $y$  is horizontal coordinate perpendicular to inductor current suppliers, 51 mm corresponds to ETP.

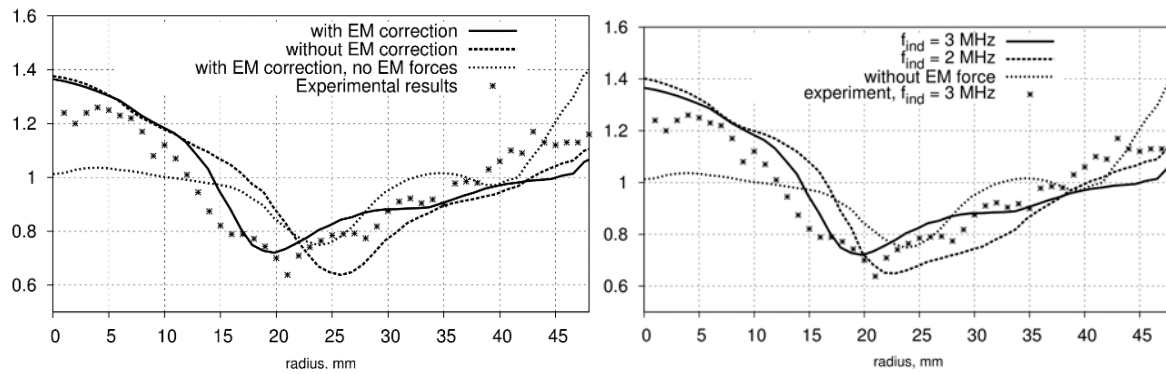


Figure 7: RRV profiles. Resistivity is normalised to its average and displayed in arbitrary units. Left:  $f_{ind} = 3$  MHz, right: calculations on the mesh obtained with EM correction.

No EM correction, $f_{ind} = 3$ MHz	With EM correction, $f_{ind} = 3$ MHz	With EM correction, no EM forces	With EM correction, $f_{ind} = 2$ MHz
0.80	0.38	0.88	0.67

Table 1. Sum of squared differences between experimental and calculated RRV profiles, in arbitrary units.

#### 4. Conclusions

It was shown that EM field has significant influence both on the shape of phase boundaries and on melt hydrodynamics. Introduced EM correction allows to describe phase boundaries more precisely, and it leads to changes in RRV profile, even although direct influence of correction on 3D HF EM field distribution is not taken into account. Position of resistivity minima became closer to experimentally observed and sum of squared differences diminished, therefore EM correction improved models' qualitative and quantitative correspondence to experiment. Experimental data for  $f_{ind} = 2$  MHz would be valuable for further validation of the mathematical models.

When calculations are performed without EM forces, distribution of velocity on melt free surface shows that Marangoni force reverses vortices near ETP. Due to the complexity of flow pattern, clear influence of the lowering of inductor current frequency cannot be detected due to intense buoyancy and Marangoni forces, which partially compensate EM forces. The next aim of the study could be implementation of EM correction in 3D HF EM calculation program, which creates EM heat sources – boundary conditions for melt flow calculations, to observe direct influence of EM correction on the 3D melt flow and dopant distribution.

#### 5. Acknowledgments

This work has been supported by the European Regional Development Fund, project Contract no. 2013/0051/2DP/2.1.1.1.0/13/APIA/VIAA/009.

#### 5. References

- [1] Lacis, K.; Muiznieks, A.; Rudevics, A.; Sabanskis, A.: Influence of DC and AC magnetic fields on melt motion in FZ large Si crystal growth. *Magnetohydrodynamics*. 46 (2010) 119-218.
- [2] Rost, H.-J.; Menzel, R.; Luedge, A.; Riemann, H.: FZ silicon crystal growth at reduced RF frequencies. *JCG*. 360 (2012) 43-46.
- [3] Ratnieks, G.; Muiznieks, A.; Muhlbauer, A.: Modelling of phase boundaries for large industrial FZ silicon crystal growth with the needle-eye technique. *JCG*. 255 (2003) 227-240.
- [4] Muiznieks, A.; Rudevics, A.; Riemann, H.; Lacis, U.: Comparison between 2D and 3D modelling of HF electromagnetic field in FZ silicon crystal growth process. *International Scientific Colloquium Modelling for Material Processing, Riga*. (2010) 61-65.